The Compton Amplitude, lattice QCD and the Feynman–Hellmann approach

K. U. Can[1], A. Hannaford-Gunn[1], R. Horsley[2*], Y. Nakamura[3], H. Perlt[4], P. E. L. Rakow[5], E. Sankey[1], G. Schierholz[6], H. Stüben[7], R. D. Young[1] and J. M. Zanotti[1]

1 CSSM, Department of Physics, University of Adelaide, Adelaide SA 5005, Australia
2 School of Physics and Astronomy, University of Edinburgh, Edinburgh EH9 3FD, UK
3 RIKEN Center for Computational Science, Kobe, Hyogo 650-0047, Japan
4 Institut für Theoretische Physik, Universität Leipzig, 04109 Leipzig, Germany
5 Theoretical Physics Division, Department of Mathematical Sciences, University of Liverpool, Liverpool L69 3BX, UK
6 Deutsches Elektronen-Synchrotron DESY, Notkestr. 85, 22607 Hamburg, Germany
7 Universität Hamburg, Regionales Rechenzentrum, 20146 Hamburg, Germany

⋆ rhorsley@ph.ed.ac.uk

*Proceedings for the XXXIII International Workshop on High Energy Physics,
Hard Problems of Hadron Physics: Non-Perturbative QCD & Related Quests
ONLINE, 8-12 November 2021*

Abstract

A major objective of lattice QCD is the computation of hadronic matrix elements. The standard method is to use three-point and four-point correlation functions. An alternative approach, requiring only the computation of two-point correlation functions is to use the Feynman-Hellmann theorem. In this talk we develop this method up to second order in perturbation theory, in a context appropriate for lattice QCD. This encompasses the Compton Amplitude (which forms the basis for deep inelastic scattering) and hadron scattering. Some numerical results are presented showing results indicating what this approach might achieve.

1 Introduction

Understanding the internal structure of hadrons and in particular the nucleon directly from the underlying QCD theory is a major task of particle physics. It is complicated because of the non-perturbative nature of the problem, and presently the only known method is to discretise QCD and use numerical Monte Carlo methods. The relevant information is encoded in correlation functions – from the all encompassing two-quark correlation functions to GTMDs, TMDs, GPDs Wigner functions, PDFs and Form Factors, e.g. [1].

Using the Operator Product Expansion (OPE), it is possible to relate form factors to moments of certain matrix elements, which in principle are calculable using lattice QCD techniques. However due to theoretical problems such as much more mixing of lattice operators due to reduced $H(4)$ symmetry and numerical problems, for many years it was only possible to compute the very lowest moments. (As an example of a complete calculation – albeit for quenched fermions – see for example [2].) This does not allow for the reconstruction of the associated PDF. Progress was recently achieved with the concepts of quasi-PDFs and pseudo-PDFs, for a comprehensive review see [3].

Here in this talk we shall describe a complementary approach which relates the structure function to that of the associated Compton amplitude, emphasising via dispersion relations the physical and unphysical regions and their connection with Minkowski and Euclidean variables. While the Compton amplitude is a correlation function it is 4-point and hence difficult to compute with the straightforward standard approach used in Lattice QCD of tying the appropriate Grassmann quark lines together in the path integral. However, we are able to circumvent this problem by using a Feynman–Hellmann approach. This approach avoids operator mixing problems, has a simple renormalisation and as independent of the Operator Product Expansion, OPE, allows an investigation of power corrections to the leading behaviour (twist 2) of the OPE. We first described this method in [4] and have been developing it further e.g. [5,6].

In this talk we give a brief introduction to this approach, first in section 2 giving the relation between structure functions and the Compton amplitude. This is followed in section 3 by a description of the Feynman–Hellmann approach. Some numerical results are given in 4.2. Further details and results are given in [5]. The Feynman–Hellmann approach is a versatile method and in the following section 5 some further applications are mentioned. Finally we give some conclusions.

2 Structure functions and the Compton amplitude

Deep Inelastic Scattering (DIS) is the inclusive scattering of a lepton (usually an electron) from nucleon (usually a proton), $eN \to e'X$. The process is shown diagrammatically in Fig. 1. The
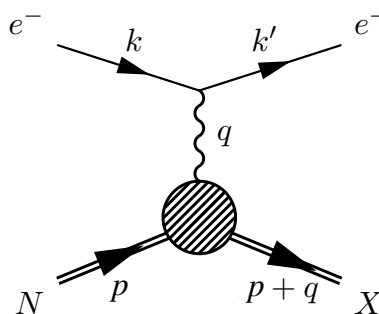
Figure 1: DIS, where k, k' represent the incoming, outgoing lepton momenta, p is the momentum of the incoming nucleon of mass M_N, $q = k - k'$ is the momentum transfer and X represents the recoiling system.

kinematics is such that $Q^2 \equiv -q^2 > 0$; the invariant mass of X is $M_X^2 = (p+q)^2$ and the Bjorken variable, x, is defined by $x = Q^2/(2p \cdot q)$. Here we shall be mainly using the inverse Bjorken variable $\omega = 1/x$. $x > 0$ from kinematics and $M_X^2 > M_N^2$ means that $x < 1$ which translates to $1 < \omega < \infty$ as the physical region. The square of the amplitude can be factorised into a

calculable leptonic tensor together with an unknown hadronic tensor, $W_{\mu\nu}$, given[1] by

$$W_{\mu\nu} \equiv \frac{1}{4\pi} \int d^4z \, e^{iq\cdot z} \rho_{ss'\,\text{rel}} \langle p, s' | [J_\mu^\dagger(z), J_\nu(0)] | p, s \rangle_{\text{rel}}, \tag{1}$$

where J_μ is the electromagnetic current (γ)[2] and for unpolarised nucleons we have $\rho_{ss'} = \delta_{ss'}/2$. The tensor has the Lorentz decomposition

$$W_{\mu\nu} = \left(-\eta_{\mu\nu} + \frac{q_\mu q_\nu}{q^2}\right) F_1(x, Q^2) + \left(p_\mu - \frac{p\cdot q}{q^2} q_\mu\right)\left(p_\nu - \frac{p\cdot q}{q^2} q_\nu\right) \frac{F_2(x, Q^2)}{p\cdot q}, \tag{2}$$

with structure functions $F_1(x, Q^2)$ and $F_2(x, Q^2)$. It is useful to relate the $W_{\mu\nu}$ scattering amplitude to the forward Compton scattering amplitude, $T_{\mu\nu}$, depicted in the LH panel of Fig. 2, as this is a correlation function and so more amenable to lattice QCD or other calculational
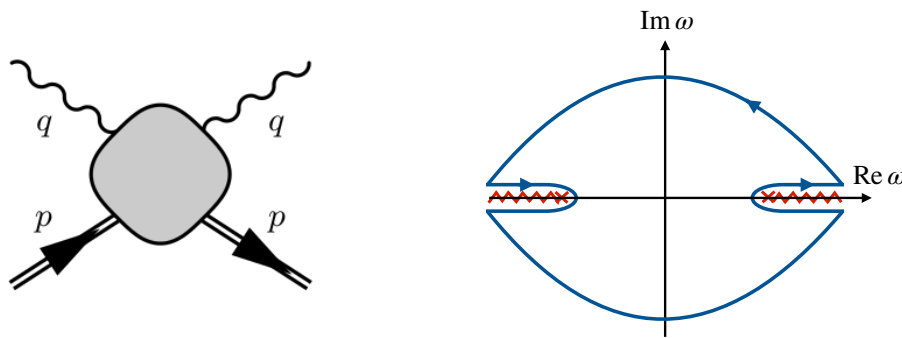
Figure 2: LH panel: The forward Compton Amplitude. RH panel: The analytic structure for $\mathcal{F}_1$ – branch cuts starting from $\omega = \pm 1$, together with the contour used for the dispersion relation.

methods. The definition parallels that of $W_{\mu\nu}$

$$T_{\mu\nu}(p, q) \equiv i \int d^4z \, e^{iq\cdot z} \rho_{ss'\,\text{rel}} \langle p, s' | T(J_\mu^\dagger(z) J_\nu(0)) | p, s \rangle_{\text{rel}}$$

$$= \left(-\eta_{\mu\nu} + \frac{q_\mu q_\nu}{q^2}\right) \mathcal{F}_1(\omega, Q^2) + \left(p_\mu - \frac{p\cdot q}{q^2} q_\mu\right)\left(p_\nu - \frac{p\cdot q}{q^2} q_\nu\right) \frac{\mathcal{F}_2(\omega, Q^2)}{p\cdot q}, \tag{3}$$

with corresponding structure functions $\mathcal{F}_1(\omega, Q^2)$, $\mathcal{F}_2(\omega, Q^2)$. Due to the time ordering in its definition it is a correlation function. These are related via the Optical theorem to the hadronic tensor structure functions by $\text{Im}\mathcal{F}_1(\omega, Q^2) = 2\pi F_1(x, Q^2)$ (and similarly for F_2, however in this talk we shall concentrate on F_1). Photon crossing symmetry $N \to \bar{N}$ means that $\mathcal{F}_1$ is symmetric under $\omega \to -\omega$ (while $\mathcal{F}_2$ is anti-symmetric). The analytic structure, e.g. [7], is thus given in the RH plot of Fig. 2. Analyticity properties (including using the Schwarz reflection principle across the branch cut) then give a once subtracted[3] dispersion relation

$$\mathcal{F}_1(\omega, Q^2) = \frac{2\omega}{\pi} \int_1^\infty d\omega' \left[\frac{\text{Im}\mathcal{F}_1(\omega', Q^2)}{\omega'(\omega' - \omega - i\epsilon)} - \frac{\text{Im}\mathcal{F}_1(\omega', Q^2)}{\omega'(\omega' + \omega - i\epsilon)} \right] + \mathcal{F}_1(0, Q^2)$$

$$= \underbrace{4\omega^2 \int_0^1 dx' \frac{x' F_1(x', Q^2)}{1 - x'^2\omega^2 - i\epsilon}}_{\overline{\mathcal{F}}_1(\omega, Q^2)} + \underbrace{\mathcal{F}_1(0, Q^2)}_{\text{once subtracted}}. \tag{4}$$

---

[1]The state normalisation is given by $_\text{rel}\langle N | N \rangle_\text{rel} = 2E_N$. See also footnote 5.
[2]This can, of course, be generalised to neutral (Z) or charged $(W^\pm)$ currents.
[3]Conventionally $\omega = 0$ is chosen as the subtraction point, but others have recently been suggested, [8].

(Replacing $x'F_1$ by F_2 with no subtraction gives the equivalent dispersion relation for F_2.) As long as we are in the unphysical region $|\omega| < 1 \Longleftrightarrow M_X^2 < M_N^2$, i.e. below elastic threshold, there is no singularity in previous integral the time ordering is irrelevant, so the $i\epsilon$ in eq. (4) can be dropped. The Minkowski and Euclidean amplitudes are then identical which as we shall see in section (3) will eventually allow a direct lattice QCD computation. Physically $|\omega| < 1$ means states propagating between currents cannot go on-shell. Taylor expanding the denominator in eq. (4) then gives

$$\overline{\mathcal{F}}_1(\omega, Q^2) = 2\sum_{n=1}^{\infty} \omega^{2n} M_{2n}^{(1)}(Q^2), \quad \text{where} \quad M_{2n}^{(1)}(Q^2) = 2\int_0^1 dx' \, x'^{2n-1} F_1(x', Q^2) \qquad (5)$$

are the Mellin moments of F_1. Furthermore for the numerical results considered later we set $\mu = \nu = z$, $p_z = q_z = 0$ giving

$$T_{33}(p, q) = \overline{\mathcal{F}}_1(\omega, Q^2) = 2\sum_{n=1}^{\infty} \omega^{2n} M_{2n}^{(1)}(Q^2). \qquad (6)$$

So from Compton amplitude data we can directly extract the Mellin moments. The positivity of the cross section means that $F_1 > 0$ or $M_2^{(1)} \geq M_4^{(1)} \geq \ldots M_{2n}^{(1)} \geq \ldots > 0$ so the expected shape of the Compton amplitude in the unphysical region for fixed Q^2 is simply an increasing polynomial function of ω^2.

3 The Feynman–Hellmann approach

The task now is to compute the (Euclidean) Compton amplitude and in particular that given in eq. (6). A direct lattice QCD computation of the path integral for the necessary 4-point correlation function is complicated as there are many diagrams to compute. As an alternative we shall use the Feynman–Hellmann approach here.

We now sketch a derivation of the procedure. Consider the 2-point nucleon correlation function

$$C_{fi\lambda}(t; \vec{p}, \vec{q}) = {}_\lambda\langle 0| \underbrace{\hat{\bar{B}}_{N_f}(0; \vec{p})}_{\text{Sink: momentum}} \hat{S}(\vec{q})^t \underbrace{\hat{\bar{B}}_{N_i}(0, \vec{0})}_{\text{Source: spatial}} |0\rangle_\lambda, \qquad (7)$$

where $\hat{S}$ is the $\vec{q}$-dependent transfer matrix $\hat{S}(\vec{q}) = \exp(-\hat{H}(\vec{q}))$ in the presence of a perturbed Hamiltonian

$$\hat{H}(\vec{q}) = \hat{H}_0 - \sum_\alpha \lambda_\alpha \hat{\bar{\mathcal{O}}}_\alpha(\vec{q}), \qquad (8)$$

where

$$\hat{\bar{\mathcal{O}}}_\alpha(\vec{q}) = \int_{\vec{x}} \left(\hat{O}_\alpha(\vec{x}) e^{i\vec{q}\cdot\vec{x}} + \hat{O}_\alpha^\dagger(\vec{x}) e^{-i\vec{q}\cdot\vec{x}} \right) \qquad (9)$$

is a Hermitian operator. λ can be taken as a real positive parameter[4]. Using time dependent perturbation theory via the Dyson Series, namely the operator expansion, regarding $\hat{B}$ as 'small'

$$e^{t(\hat{A}+\hat{B})} = e^{t\hat{A}} + \int_0^t dt' \, e^{(t-t')\hat{A}} \hat{B} \, e^{t'\hat{A}} + \int_0^t dt' \int_0^{t'} dt'' \, e^{(t-t')\hat{A}} \hat{B} \, e^{(t'-t'')\hat{A}} \hat{B} e^{t''\hat{A}} + O(\hat{B}^3), \quad (10)$$

---

[4] Can generalise to complex λ by absorbing the phase into the operator: $\lambda_\alpha \hat{O}_\alpha(\vec{x}) \to |\lambda_\alpha| e^{i\phi_\alpha} \hat{O}_\alpha(\vec{x})$.

and inserting complete sets of unperturbed states[5]

$$|N(\vec{p})\rangle\langle N(\vec{p})| + \sum_{E_X(\vec{p}_X)>E_N(\vec{p})} |X(\vec{p}_X)\rangle\langle X(\vec{p}_X)| = 1, \tag{11}$$

appropriately gives after some algebra the factorised result

$$C_{fi\lambda}(t;\vec{p},\vec{q}) = {}_\lambda\langle 0|\hat{\bar{B}}_{N_f}(\vec{p})|N(\vec{p})\rangle \times {}_\lambda\langle N(\vec{p})|\hat{\bar{B}}_{N_i}(\vec{0})|0\rangle_\lambda \times e^{-E_{N\lambda}(\vec{p},\vec{q})t} + \dots, \tag{12}$$

where as this equation suggests we have taken the lowest state $|N(\vec{p})\rangle$ to be well separated from other states. Furthermore we have defined ${}_\lambda\langle N(\vec{p})|$ as

$$_\lambda\langle N(\vec{p})| = \langle N(\vec{p})| + \lambda_\alpha \sum_{E_Y(\vec{p}_Y)>E_N(\vec{p})} \frac{\langle N(\vec{p})|\hat{\bar{\mathcal{O}}}_\alpha(\vec{q})|Y(\vec{p}_Y)\rangle}{E_Y(\vec{p}_Y)-E_N(\vec{p})}\langle Y(\vec{p}_Y)| + O(\lambda^2). \tag{13}$$

(We do not give the $O(\lambda^2)$ term here.) While the final nucleon operator, $\hat{\bar{B}}_{N_f}(\vec{p})$, has a definite momentum and so just picks out one state, the initial nucleon operator, $\hat{B}_{N_i}(\vec{0})$, being at position $\vec{x}=\vec{0}$ contains all momenta and states (indicated here by the sum over $|X(\vec{p}_X)\rangle$). For the matrix elements that appear in the modified energy in eq. (12), rather than writing them in terms of the operator $\hat{\bar{\mathcal{O}}}_\alpha$ we first use $\hat{O}(\vec{x}) = e^{-i\hat{\vec{p}}\cdot\vec{x}}\hat{O}(\vec{0})e^{i\hat{\vec{p}}\cdot\vec{x}}$ on the relevant term to give

$$\langle X(\vec{p}_X)|\hat{\bar{\mathcal{O}}}_\alpha(\vec{q})|N(\vec{p})\rangle = \langle X(\vec{p}_X)|\hat{O}_\alpha(\vec{0})|N(\vec{p})\rangle\,\delta_{\vec{p}_X,\vec{p}+\vec{q}} + \langle X(\vec{p}_X)|\hat{O}_\alpha^\dagger(\vec{0})|N(\vec{p})\rangle\,\delta_{\vec{p}_X,\vec{p}-\vec{q}}, \tag{14}$$

so matrix elements step up or down in $\vec{q}$. As this is also valid for $X = N$ then the $O(\lambda)$ term[6] vanishes ($\vec{q}\neq\vec{0}$). Generalising each λ inserts another $\hat{\bar{\mathcal{O}}}$ into the matrix element, so we need an even number of λs, i.e. odd powers of λ vanish. This gives finally

$$\begin{aligned} E_{N\lambda}(\vec{p},\vec{q}) = E_N(\vec{p}) - \sum_{E_X(\vec{p}\pm\vec{q})>E_N(\vec{p})} &\left[\frac{|\langle X(\vec{p}+\vec{q})|\lambda_\alpha\hat{O}_\alpha(\vec{0})|N(\vec{p})\rangle|^2}{E_X(\vec{p}+\vec{q})-E_N(\vec{p})} \right. \\ &\left. + \frac{|\langle X(\vec{p}-\vec{q})|(\lambda_\alpha\hat{O}_\alpha(\vec{0}))^\dagger|N(\vec{p})\rangle|^2}{E_X(\vec{p}-\vec{q})-E_N(\vec{p})} \right] + O(\lambda^3). \end{aligned} \tag{15}$$

We need $E_N(\vec{p}\pm\vec{q}) > E_N(\vec{p})$ ($X = N$ is the worst case) giving $-1 < \omega < 1$ with $\omega = 2\vec{p}\cdot\vec{q}/\vec{q}^2$. This is the usual definition of ω (with $q_0 = 0$), which is in the safe unphysical region.

What has all this to do with the Compton Amplitude? We now interpret this result and relate it to the Compton Amplitude. Considering its Minkowski ($\mathcal{M}$) definition again, eq. (3), and again inserting a complete set of states for $t > 0$ and $t < 0$ with the appropriate $i\epsilon$ prescription

$$\begin{aligned} T_{\mu\nu}^{(\mathcal{M})}(p,q) = \sum_X &\left[\frac{\langle X(\vec{p}+\vec{q})|\hat{O}_\mu(\vec{0})|N(\vec{p})\rangle^* \langle X(\vec{p}+\vec{q})|\hat{O}_\nu(\vec{0})|N(\vec{p})\rangle}{E_X(\vec{p}+\vec{q})-E_N(\vec{p})-q^0-i\epsilon} \right. \\ &\left. + \frac{\langle X(\vec{p}-\vec{q})|\hat{O}_\nu^\dagger(\vec{0})|N(\vec{p})\rangle^* \langle X(\vec{p}-\vec{q})|\hat{O}_\mu^\dagger(\vec{0})|N(\vec{p})\rangle}{E_X(\vec{p}-\vec{q})-E_N(\vec{p})+q^0-i\epsilon} \right]. \end{aligned} \tag{16}$$

Comparing with the previous result of eq. (15) if we set $q^0 = 0$ and choose the $\vec{p},\vec{q}$ geometry so that $E_X(\vec{p}\pm\vec{q}) > E_N(\vec{p})$, i.e. $-1 < \omega < 1$ then we can also drop the $i\epsilon$ which gives

$$E_{N\lambda}(\vec{p},\vec{q}) = E_N(\vec{p}) - \frac{\lambda_\alpha^*\lambda_\beta}{{}_{\mathrm{rel}}\langle N(\vec{p})|N(\vec{p})\rangle_{\mathrm{rel}}} T_{\alpha\beta}^{(\mathcal{M})}((E_N(\vec{p}),\vec{p}),(0,\vec{q})) + O(\lambda^4). \tag{17}$$

---

[5]The lattice normalisation is used here: $\langle X(\vec{p}_X)|Y(\vec{p}_Y)\rangle = \delta_{XY}\delta_{\vec{p}_X\vec{p}_Y}$. To convert to the usual relativistic normalisation, with an additional factor $2E_X$, change $|X\rangle \to |X\rangle/\sqrt{\langle X|X\rangle}$ with $|0\rangle \to |0\rangle$.

[6]Namely $-\lambda_\alpha\langle N(\vec{p})|\hat{\bar{\mathcal{O}}}_\alpha(\vec{q})|N(\vec{p})\rangle$.

As $T_{\alpha\beta}^{(\mathcal{M})}(p,q)^* = T_{\beta\alpha}^{(\mathcal{M})}(p,q)$ then the real part of Compton amplitude is symmetric (unpolarised case with λ real) while the imaginary part is anti-symmetric (polarised with λ complex).

For the DIS case considered here in eq. (6) where $\mu = \nu = z$; $p_z = q_z = 0$, giving $T_{33}(p,q) = \mathcal{F}_1(\omega, Q^2)$. So with $O_\alpha \to J_z$ we have finally

$$\Delta E_{N\lambda}(\vec{p}, \vec{q}) \equiv E_{N\lambda}(\vec{p}, \vec{q}) - E_N(\vec{p}) = -\frac{\lambda_z^2}{2E_N(\vec{p})} \mathcal{F}_1(\omega, Q^2) + O(\lambda^4), \tag{18}$$

writing the relativistic normalisation explicitly.

4 The Lattice

We now briefly describe some lattice details. In the Lagrangian in the path integral we add the equivalent perturbation

$$\mathcal{L}(x) = \mathcal{L}_0(x) + 2\lambda_z \cos(\vec{q} \cdot \vec{x}) J_z(x), \tag{19}$$

where rather than considering the complete electromagnetic current we take the vector current $J_\mu^{(q)}$ to be either $Z_V \bar{u}\gamma_\mu u$ (where $q \to u$) or $Z_V \bar{d}\gamma_\mu d$ ($q \to d$). Z_V has been previously determined. We only modify the propagators for the valence u/d quarks in λ. So there are no quark-line disconnected terms considered here. To include this would require at least very expensive dedicated configuration generation.

More specifically we consider 2+1 quark mass degenerate flavours on a $N_S^3 \times N_T = 32^3 \times 64$ lattice with a spacing $a \sim 0.074$ fm. (Technically $\beta = 5.50$, $\kappa_l = 0.120900$, $l = u$, d or s giving $m_\pi \sim 470$ MeV and $m_\pi L \sim 5.4$ where $L = aN_S$.) For more details of the action and configuration generation see [9]. Apart from $\lambda_z = 0$, we use 4 values of λ_z, namely ± 0.0125, ± 0.025. Q^2 has 5 values in the range between 3 and 7 GeV^2 and we make $\sim O(10^4)$ measurements for each λ_z, Q^2 pair (varying $\vec{p}$ is numerically cheap as it is not part of the source, and hence not connected with the numerically expensive fermion matrix inversion).

4.1 Kinematic coverage

We now briefly discuss the possible kinematic coverage, which is sketched in the LH panel of Fig 3. As an example consider fixed $\vec{q} = (2\pi/L)(3,5,0)$. We can access different ω by varying
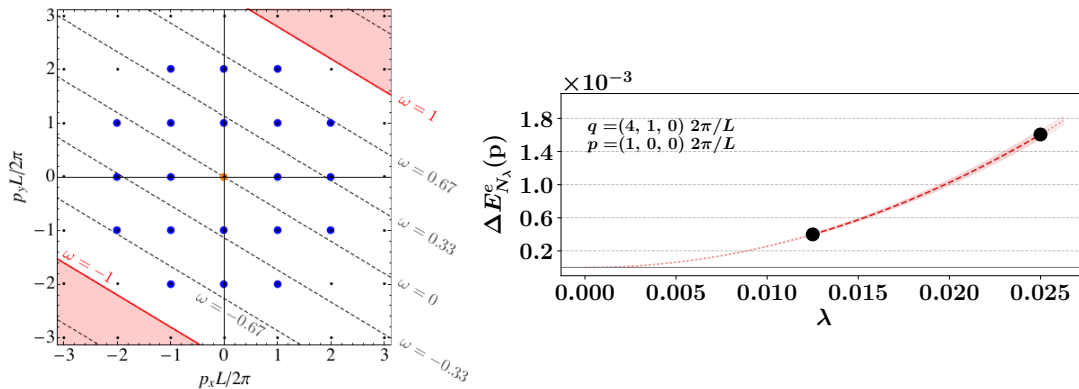
Figure 3: LH panel: The allowed kinematic possibilities for $\vec{p}$ given $\vec{q} = 2\pi/L(3,5,0)$, where $L = 32a$. Lines of constant $\omega = (2/34)(3n_x + 5n_y)$ are shown dashed. The blue dots give the allowed momenta. RH panel: A plot of $\Delta E_{N\lambda}$ against λ_z for $\vec{q} = 2\pi/L(4,1,0)$ and $\vec{p} = 2\pi/L(1,0,0)$.

the nucleon momenta $\vec{p} = (2\pi/L)\vec{n}$ as $\omega = 2\vec{p} \cdot \vec{q}/\vec{q}^2 = (2/34)(3n_x + 5n_y)$. Thus for a given constant ω we have a linear relationship between n_y and n_x as shown by the lines in the LH panel of Fig. 3. The blue dots give allowed values of $\vec{p}$.

To extract energy shifts, $\Delta E_{N\lambda}$, for each λ_z we form ratios, R_λ which isolate the $O(\lambda_z^2)$ term

$$R_\lambda = \frac{C_{NN+\lambda_z}(t) \, C_{NN-\lambda_z}(t)}{C_{NN\,0}(t)^2} = A_\lambda(\vec{p}, \vec{q}) \, e^{-2\Delta E_{N\lambda}(\vec{p}, \vec{q})} + \dots . \tag{20}$$

After extracting $\Delta E_{N\lambda}$, this is plotted against λ_z. An example is shown in the RH panel of Fig. 3 for $\vec{q} = 2\pi/L(4, 1, 0)$, $\vec{p} = 2\pi/L(1, 0, 0)$ (giving $Q^2 = 4.7\,\text{GeV}^2$). A quadratic fit gives from eq. (18) the structure function, $\mathcal{F}_1(\omega, Q^2)$, at one value of ω. Repeating this for various values of $\vec{p}$ and $\vec{q}$ gives the complete structure function of ω and Q^2.

4.2 Results

In Fig. 4 we show $\mathcal{F}_1(\omega, Q^2)$ as a function of ω for $Q^2 = 4.7\,\text{GeV}^2$ for $J_z^{(u)}$ and $J_z^{(d)}$ separately.
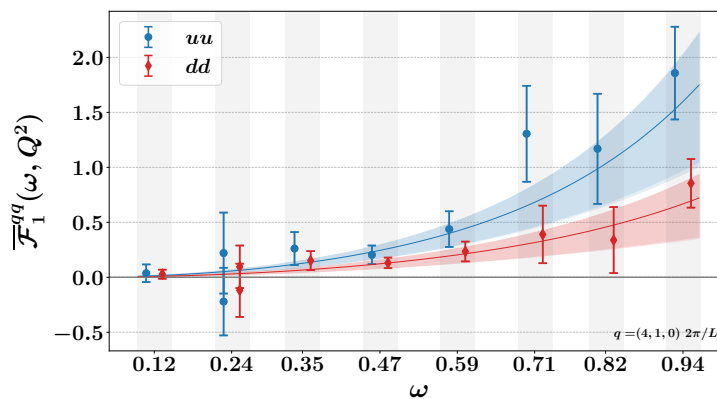
Figure 4: ω dependence of $\mathcal{F}_1(\omega, Q^2)$ for $Q^2 = 4.7\,\text{GeV}^2$. The blue circles are for $J_z^{(u)}$, the red diamonds for $J_z^{(d)}$. The fits, blue and red lines with errors given by shaded region are described in the text. The points are slightly shifted for clarity.

This figure is our main result. We now mention some further consequences from this result. From eq. (5) we can make a fit to $\mathcal{F}_1(\omega, Q^2)$ to determine the (low) Mellin moments. We have the constraints $M_2^{(1)} \geq M_4^{(1)} \geq \dots \geq M_{2n}^{(1)} \geq \dots > 0$ for u, d separately and so we have implemented a Bayesian procedure (likelihood with priors as constraints). These are also shown in the LH panel of Fig. 5 for $n = 6$. We note that the fall-off of the moments is as expected, however the second moment does not decrease as rapidly as expected from DIS.

Alternatively we can investigate the Q^2 dependence of a particular moment and investigate scaling and the existence of power corrections not restricted to the OPE and large Q^2 as shown in the RH panel of Fig. 5. We also made the naive fit

$$M_{2;u-d}^{(1)}(Q^2) = M_{2;u-d}^{(1)} + \frac{C_2^{(u-d)}}{Q^2} . \tag{21}$$

We concluded, [5, 10, 11], that we need $Q^2 \gtrsim 16\,\text{GeV}^2$ to reliably extract moments at a scale of $\mu = 2\,\text{GeV}$.

Is it possible to reconstruct the Form Factor, F_1 or indeed the PDF? This, of course, would be the ultimate goal. From eq. (4) we have

$$T_{33}(\omega, Q^2) = \omega \int_0^1 dx \, K(x\omega) F_1(x, Q^2), \quad \text{where} \quad K(\xi) = 4\frac{\xi}{1 - \xi^2} . \tag{22}$$
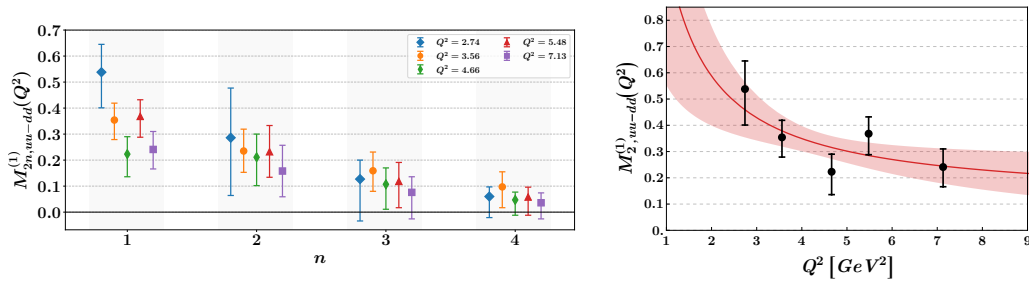
Figure 5: LH panel: The first 5 isovector moments $M^{(1)}_{2n;u-d}(Q^2)$ (using $J^{(u)}_z - J^{(d)}_z$ for various Q^2 values). RH panel: The corresponding valence PDF for $M^{(1)}_{2;u-d}(Q^2)$ $Q^2 = 2.7\,\text{GeV}^2$, together with the fit from eq. (21).

This is a Fredholm integral equation and so an inverse problem, which is ill defined. Presently with this data, we have first made the ansatz

$$F_1(x, Q^2) \equiv a\, p_{\text{val}}(x; b, c) = a\, \frac{\Gamma(b + c + 3)}{\Gamma(b + 2)\Gamma(c + 1)}\, x^b (1 - x)^c, \tag{23}$$

(normalised to $\int_0^1 dx\, x\, p_{\text{val}} = 1$). Again with a Bayesian implementation, we find typical results as in Fig. 6 here for $Q^2 = 2.7\,\text{GeV}^2$. The general shape is okay (the parton model would give
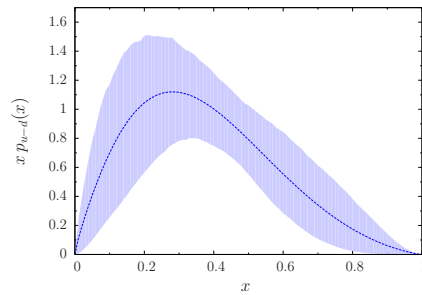
Figure 6: The valence PDF, $p^{(u-d)}_{\text{val}}$ for $Q^2 = 2.7\,\text{GeV}^2$.

a δ-function at $x = 1/3$, which is smeared out by QCD corrections).

5 Further applications

Finally we briefly mention some more applications of this method.

5.1 The $O(\lambda)$ term

We previously showed that the $O(\lambda)$ terms vanish if $\vec{q} \neq \vec{0}$. However for $\vec{q} = \vec{0}$ then it is possible to determine the baryon charges. For example in [12] the tensor charge of octet baryons was determined.

However we can escape this constraint if there is an degeneracy when two (or more) states have the same energy. Then we now have a matrix of states $M_{rs} = \langle N(\vec{p}_r)|\hat{\tilde{O}}(\vec{q})|N(\vec{p}_s)\rangle$ (where $r, s = 1, \ldots, d_S$, where d_S is the number of degenerate states). As before the diagonal elements vanish, but the off-diagonal do not. This can be diagonalised to give $\Delta E_{N\lambda}$. In [13] this was investigated (for $d_S = 2$ in the Breit frame) and applied to form factors and scattering over a large range of Q^2.

5.2 The $O(\lambda^2)$ term

While most of our present effort has been directed at the forward Compton amplitude, we have also started to investigate Off-forward Compton Amplitude (OFCA) and GPDs in [14] where we described the fomalism and determined the two lowest moments.

5.3 Possible future perspectives

Possible future perspectives include Spin dependent Structure functions and Form factors as indicated in eq. (17), electromagnetic corrections to the proton – neutron mass splitting $M_p - M_n = \delta M^\gamma + \delta M^{m_d - m_u}$ via the Cottingham formula

$$\delta M^\gamma = \frac{i}{2M} \frac{\alpha_{em}}{(2\pi)^2} \int \frac{\eta^{\mu\nu}}{q^2 + i\epsilon} T_{\mu\nu}(p, q), \tag{24}$$

and mixed currents, for example neutrino-nucleon charged weak current $\nu N \to eX$ or $eN \to \nu X$

$$
\begin{aligned}
W^{\mu\nu} &\equiv \frac{1}{4\pi} \int d^4 z \, e^{iq \cdot z} \rho_{ss' \, \text{rel}} \langle p, s' | [J^\mu_{\text{em}}(z), J^\nu_{W,A}(0)] | p, s \rangle_{\text{rel}} \\
&= -i\epsilon^{\mu\nu\alpha\beta} \frac{q_\alpha P_\beta}{2p \cdot q} F_3(x, Q^2),
\end{aligned}
\tag{25}
$$

where $J^\nu_{W,A} = \bar{u}\gamma_\nu\gamma_5 d$ the axial part of the weak charged current.

A potential problem is including quark-line-disconnected matrix elements. This needs purpose generated configurations with the fermion determinant also containing the λ term. For (H)MC for the probability definition of the action also need a real determinant so fermion matrix must be γ_5-Hermitian which means that λ^V and λ^A have to be imaginary (while λ^S, λ^P and λ^T are all real). In this case ΔE_λ develops an imaginary part. (This is not a problem for the valence sector, as this is just an inversion of a matrix.) Simulations are however possible and this was investigated in [15] (at $O(\lambda)$) for the disconnected contributions to the spin of the nucleon.

6 Conclusions

We have described here a new versatile approach for the computation of matrix elements only involving computation of 2-point correlation functions rather than 3-pt or 4-pt which is able to compute Compton amplitudes and structure function moments. Advantages include longer source-sink separations – so less excited states contamination and overcoming fierce operator mixing / renormalisation issues.

Acknowledgements

The numerical configuration generation (using the BQCD lattice QCD program [16])) and data analysis (using the Chroma software library [17]) was carried out on the DiRAC Blue Gene Q and Extreme Scaling (EPCC, Edinburgh, UK) and Data Intensive (Cambridge, UK) services, the GCS supercomputers JUQUEEN and JUWELS (NIC, Jülich, Germany) and resources provided by HLRN (The North-German Supercomputer Alliance), the NCI National Facility in Canberra, Australia (supported by the Australian Commonwealth Government) and the Phoenix HPC service (University of Adelaide). RH is supported by STFC through grant ST/P000630/1. HP is supported by DFG Grant No. PE 2792/2-1. PELR is supported in part by the STFC under

contract ST/G00062X/1. GS is supported by DFG Grant No. SCHI 179/8-1. RDY and JMZ are supported by the Australian Research Council grant DP190100297.

References

[1] M. Diehl, *Introduction to GPDs and TMDs*, Eur. Phys. J. A **52**, 149 (2016), doi:10.1140/epja/i2016-16149-3, [arXiv:1512.01328].

[2] M. Göckeler, R. Horsley, D. Pleiter, P. E. L. Rakow and G. Schierholz, *A lattice determination of moments of unpolarized nucleon structure functions using improved Wilson fermions*, Phys. Rev. D **71**, 114511 (2005), doi:10.1103/PhysRevD.71.114511, [arXiv:hep-ph/0410187].

[3] K. Cichy and M. Constantinou, *A Guide to Light-Cone PDFs from Lattice QCD: An Overview of Approaches, Techniques, and Results*, Adv. High Energy Phys. 3036904 (2019), doi:10.1155/2019/3036904, [arXiv:1811.07248].

[4] A. J. Chambers et al., *Nucleon Structure Functions from Operator Product Expansion on the Lattice*, Phys. Rev. Lett. **118**, 242001 (2017), doi:10.1103/PhysRevLett.118.242001, [arXiv:1703.01153].

[5] K. U. Can et al., *Lattice QCD evaluation of the Compton amplitude employing the Feynman-Hellmann theorem*, Phys. Rev. D **102**, 114505 (2020), doi:10.1103/PhysRevD.102.114505, [arXiv:2007.01523].

[6] K. U. Can et al., *Investigating the low moments of the nucleon structure functions in lattice QCD*, arXiv:2110.01310.

[7] S. Gasiorowicz, *Elementary Particle Physics*, Wiley (1966).

[8] F. Hagelstein and V. Pascalutsa, *The subtraction contribution to the muonic-hydrogen Lamb shift: A point for lattice QCD calculations of the polarizability effect*, Nucl. Phys. A **1016**, 122323 (2021), doi:10.1016/j.nuclphysa.2021.122323, [arXiv:2010.11898].

[9] W. Bietenholz et al., *Flavor blindness and patterns of flavor symmetry breaking in lattice simulations of up, down, and strange quarks*, Phys. Rev. D **84**, 054509 (2011), doi:10.1103/PhysRevD.84.054509, [arXiv:1102.5300].

[10] R. Horsley et al., *Structure functions from the Compton amplitude*, Proc. Sci. **363**, 137 (2020), doi:10.22323/1.363.0137, [arXiv:2001.05366].

[11] A. Hannaford-Gunn et al., *Scaling and higher twist in the nucleon Compton amplitude*, Proc. Sci. **363**, 278 (2020), doi:10.22323/1.363.0278, [arXiv:2001.05090]

[12] R. E. Smail et al., *Tensor Charges and their Impact on Physics Beyond the Standard Model*, Proc. Sci. **LATTICE2021**, 494 (2021), arXiv:2112.05330.

[13] A. J. Chambers et al., *Electromagnetic form factors at large momenta from lattice QCD*, Phys. Rev. D **96**, 114509 (2017), doi:10.1103/PhysRevD.96.114509, [arXiv:1702.01513].

[14] A. Hannaford-Gunn et al., *Generalized parton distributions from the off-forward Compton amplitude in lattice QCD*, Phys. Rev. D **105**, 014502 (2022), doi:10.1103/PhysRevD.105.014502, [arXiv:2110.11532].

[15] A. J. Chambers et al., *Disconnected contributions to the spin of the nucleon*, Phys. Rev. D **92**, 114517 (2015), doi:10.1103/PhysRevD.92.114517, [arXiv:1508.06856].

[16] T. R. Haar, Y. Nakamura and H. Stüben, *An update on the BQCD Hybrid Monte Carlo program*, EPJ Web Conf. **175**, 14011 (2018), doi:10.1051/epjconf/201817514011, [arXiv:1711.03836].

[17] R. G. Edwards and B. Joó, *The Chroma Software System for Lattice QCD*, Nucl. Phys. B Proc. Suppl. **140**, 832 (2005), doi:10.1016/j.nuclphysbps.2004.11.254, [arXiv:hep-lat/0409003].